

Direct observation of delithiation as the origin of analog memristance in Li_xNbO_2

Sebastian A. Howard,¹ Christopher N. Singh,¹ Galo J. Paez,¹ Matthew J. Wahila,¹ Linda W. Wangoh,¹ Shawn Sallis,² Keith Tirpak,¹ Yufeng Liang,³ David Prendergast,³ Mateusz Zuba,¹ Jatinkumar Rana,¹ Alex Weidenbach,⁴ Timothy M. McCrone,⁴ Wanli Yang,⁵ Tien-Lin Lee,⁶ Fanny Rodolakis,⁷ William Doolittle,⁴ Wei-Cheng Lee,¹ and Louis F. J. Piper^{1,2, a)}

¹⁾*Department of Physics, Applied Physics and Astronomy, Binghamton University, Binghamton, New York 13902, USA*

²⁾*Materials Science & Engineering, Binghamton University, Binghamton, New York 13902, USA*

³⁾*The Molecular Foundry, Lawrence Berkeley National Laboratory, Berkeley, California 94720, USA*

⁴⁾*School of Electrical and Computer Engineering, Georgia Institute of Technology, Atlanta, GA, 30332, USA*

⁵⁾*Advanced Light Source, Lawrence Berkeley National Laboratory, Berkeley, California 94720, USA*

⁶⁾*Diamond Light Source Ltd., Harwell Science and Innovation Campus, Didcot, Oxfordshire OX11 0DE, UK*

⁷⁾*Argonne National Laboratory, 9700 South Cass Avenue, Argonne, IL 60439, USA*

(Dated: 4 June 2019)

The discovery of analog Li_xNbO_2 memristors revealed a promising new memristive mechanism wherein the diffusion of Li^+ rather than O^{2-} ions enables precise control of the resistive states. However, directly correlating lithium concentration with changes to the electronic structure in active layers remains a challenge and is required to truly understand the underlying physics. Chemically delithiated single crystals of LiNbO_2 present a model system for correlating lithium variation with spectroscopic signatures from operando soft x-ray spectroscopy studies of device active layers. Using electronic structure modeling of the x-ray spectroscopy of Li_xNbO_2 single crystals, we demonstrate that the intrinsic memristive behavior in Li_xNbO_2 active layers results from field-induced degenerate p -type doping. We show that electrical operation of Li_xNbO_2 -based memristors is viable even at marginal Li deficiency and that the analog memristive switching occurs well before the system is fully metallic. This study serves as a benchmark for material synthesis and characterization of future Li_xNbO_2 -based memristor devices, and suggests that valence change switching is a scalable alternative that circumvents the electroforming typically required for filamentary-based memristors.

INTRODUCTION

Functional oxide memristors have the potential to revolutionize neuromorphic computing, which aims to mimic the operation of biological brains using artificial circuits.^{1,2} While neuromorphic systems can be implemented with traditional CMOS circuitry, this requires a large number of conventional transistors, resulting in significant power consumption and scalability issues.³⁻⁵ In contrast, truly biomimetic circuits would lead to scalable, low-power processors capable of hardware-level autonomous learning, power-efficient image recognition, and other exciting possibilities.^{6,7} Neuristor circuits based on functional oxide memristors have the potential to enable these truly biomimetic circuits. However, the resistive switching of these memristors is typically attributed to a complex combination of processes (e.g., redox reactions, ionic transport, phase changes, etc.),⁸ which are highly dependent on device architecture and are not yet fully understood.^{9,10}

Lithium niobate (Li_xNbO_2), which has been previously studied due to properties such as superconductivity,¹¹ has recently shown great potential for memristive applications.^{12,13} Whereas traditional filamentary devices typically require the migration of O^{2-} ions to form narrow conductive channels and access discrete resistive states, the resistive states of Li_xNbO_2 are analog in nature and are thought to be modulated by a more uniform diffusion of Li^+ ions throughout the active layer.¹⁴ This more uniform ion diffusion mechanism may help to overcome some of the major disadvantages of traditional memristors, such as the need for an initial pre-forming/electroforming process to breakdown or otherwise alter the as-deposited material before the device can function.¹⁵ In addition, many sources of device

^{a)}Electronic mail: lpiper@binghamton.edu

failure, such as thermal stress from conduction through nanoscale pathways, non-uniform O^{2-} ion clustering, or other failure modes,¹⁶ may be completely absent in these $LiNbO_2$ -based devices. Further investigation of these $LiNbO_2$ memristors is therefore needed to fully characterize this promising memristive mechanism.

It has been proposed that the electronic properties of Li_xNbO_2 are highly dependent on the Li^+ content, and that a bias-induced Li-gradient could enable precise control of the resistive state.¹⁷ This bias-induced Li gradient was previously investigated across an annular $LiNbO_2$ device using spatially resolved in-situ oxygen K-edge x-ray absorption spectroscopy,¹⁴ revealing gradual changes in the spectral lineshape across the active layer interpreted as lithium concentration variations. Recent advances in x-ray absorption simulations of the O K-edge¹⁸ have now presented an opportunity to confirm the predicted evolution of Li_xNbO_2 within these devices and accurately describe their operational mechanism.

In this paper, we benchmark the intrinsic material properties responsible for the analog memristive behavior of Li_xNbO_2 . High-quality single crystals were grown using liquid phase electro-epitaxy and then chemically delithiated for direct comparison to atomistic modeling. Li_xNbO_2 single crystals with well-defined lithium concentrations were preferred over active layer thin films in order to disentangle the effects of Li content variation from other phenomenon. Soft and hard x-ray spectroscopy techniques, as well as first-principles x-ray spectroscopic simulations, were used to monitor the niobium coordination and electronic structure evolution of Li_xNbO_2 . Using x-ray absorption spectroscopy, we were then able to confirm the depopulation of the Nb $4d_{z^2}$ orbital upon Li^+ ion extraction, considered responsible for the memristive behavior. The excellent agreement between theory and experiment allows us to explain the electronic structure evolution of Li_xNbO_2 up to $x = 0.5$, i.e., degenerate p -type semiconductor regime (above which the Li_xNbO_2 is metallic). After reexamining previous *in-situ* oxygen K-edge x-ray absorption measurements of Li_xNbO_2 ,¹⁴ we conclude that the analog memristive switching in the devices occurs within the degenerate p -doping regime rather than being associated with a full insulator-to-metal transition.

EXPERIMENTAL DETAILS

$LiNbO_2$ single crystals were grown using a liquid phase electro-epitaxy (LPEE) method. The LPEE growth method makes use of Nb_2O_5 (99.9%) and $LiBO_2$ (99.9%). The $LiNbO_2$ crystals were grown over a 24 hour period and nucleated on a niobium rod at 1.1 V with a 10:1 $LiBO_2$ to Nb_2O_5 ratio. Some $LiNbO_2$ crystals were delithiated in a 37% HCl aqueous bath at room temperature for 24 hours followed by a rinse with DI water, and then dried with nitrogen. Other crystals were set aside to act as pristine references, while some large crystals were reserved for device fabrication. To create the memristor devices, 100 nm of Ti and 500 nm of Au were deposited on the large crystals using evaporation and then patterned into device contacts using a lift-off process. These volatile ring dot devices were then tested with IV sweeps. Initial scans were performed to find minimum programming voltage starting at 0.1 V and increasing in steps of 0.1 V, followed by a collection of data at minimum programming voltage.¹⁹

Some crystals were ball milled or ground manually using a mortar and pestle for powder measurements. X-ray diffraction (XRD) was performed on powdered $LiNbO_2$ using a Bruker D8 Advance diffractometer with Bragg-Brentano geometry and a Cu K_α source at Georgia Institute of Technology. Phase identification was performed using Bruker DIFFRAC.EVA software coupled with the PDF-2016 database. X-ray absorption near edge structure (XANES) and extended x-ray absorption fine structure (EXAFS) measurements were also performed on powdered $LiNbO_2$ to determine the effective Nb oxidation state in the bulk, as well as local electronic/atomic structure. The XANES and EXAFS were performed at beamline 20-BM of the Advanced Photon Source at Argonne National Laboratory in Lemont, IL (see section I A. of the supplementary material).

Soft and hard x-ray photoelectron spectroscopy (XPS and HAXPES), which have an effective probing depth of ~ 4 nm (surface) and ~ 15 nm (sub-surface), respectively, were performed on $LiNbO_2$ crystals to determine the Li content, Nb oxidation state, and the valence band electronic structure. In addition, x-ray absorption spectroscopy (XAS) measurements of the oxygen K-edge were performed in total electron yield (TEY) mode, which can probe up to 5 nm deep.²⁰ The HAXPES was performed at beamline I09 of the Diamond Light Source at the Harwell Science and Innovation Campus in Oxfordshire, UK, while variable photon energy XPS and XAS was performed at beamline 29-ID of the Advanced Photon Source at Argonne National Laboratory in Lemont, IL. Some additional XPS was performed at the Analytical and Diagnostics Laboratory at Binghamton University, while additional XAS was performed at beamline 8 of the Advanced Light Source at Lawrence Berkeley National Laboratory in Berkeley, CA (see sections I A and B. of the supplementary material).

Density functional theory (DFT) electronic ground state calculations at various Li concentrations were performed within the Vienna Ab Initio Simulation (VASP) package,²¹ (see section I C. of the supplementary material). The x-ray formalism of the core-hole approach for simulating the O k-edge in pristine and delithiated cases was performed within the ShirleyXAS + MBXASPY environment.^{18,22-24} The DFT information of the x-ray final state was obtained using full core-hole (FCH) approach in which an electron is removed from the inner shell of a designated excited atom within

a supercell. Therefore, the interaction between the core hole and the electron was not explicitly included via many-body approaches, such as the Feynman diagram technique, but was instead accounted for using a modified oxygen pseudo-potential with one electron removed from the 1s orbital for the O K-edge. The excited electron was then added to the occupied electronic structure. Next, the modified electronic system was relaxed to its ground state using DFT. Finally, the initial-state and final-state DFT orbitals and energies were provided as input for the MBXASPY software codes to produce the determinant spectra. We utilized a $1 \times 1 \times 1$ supercell structure for the rutile and BCT NbO_2 calculations, as well as the $\text{Li}_{0.5}\text{NbO}_2$. The fully lithiated LiNbO_2 was calculated using a $3 \times 3 \times 1$ supercell. All supercells were chosen such that their dimensions were large enough to avoid effects due to neighboring periodic images.

RESULTS AND DISCUSSION

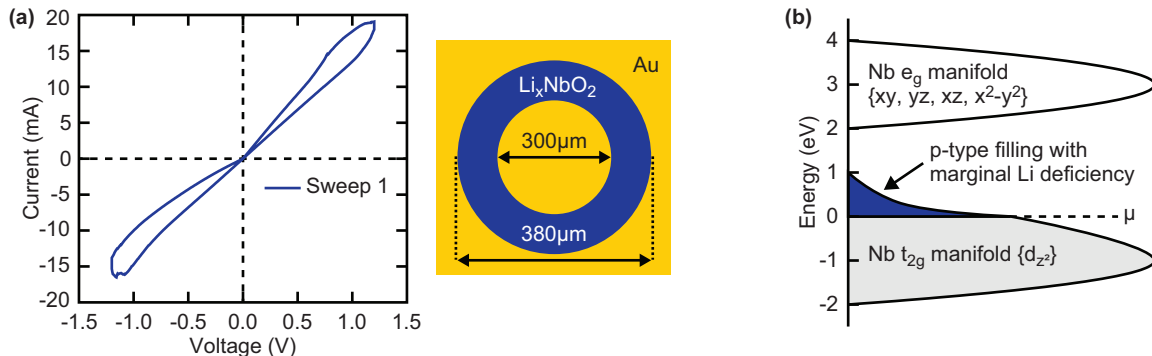


FIG. 1. (a) The IV Sweep (left) of a ring dot memristor device (right) fabricated using a Li_xNbO_2 crystal grown via liquid phase electro-epitaxy. (b) A schematic band diagram depicting the niobium valence manifold reacting to Li deficiency. Oxygen $2p$ character forms only $\approx 10\%$ of the bands at this energy, and so are omitted for clarity.

A representative pinched hysteresis IV curve taken on a high-quality, single crystal LiNbO_2 ring dot memristor is shown in Figure 1(a), consistent with previous reports of analog memristive behavior for LiNbO_2 .^{19,25} Since the crystals show similar IV curve responses to LiNbO_2 devices grown via both molecular beam epitaxy^{12,14} and sputter deposition²⁶, we consider the underlying mechanism to be inherent to the material rather than the device processing. As such, chemically delithiated LiNbO_2 single crystals should display the same electronic structure modifications as those electrochemically induced in the thin film devices.

As shown in Figure 1(b), the chemical potential (μ) is expected to lower into the Nb $4d_{z^2}$ -derived valence band as lithium is extracted, thereby favoring hole formation (p -type). Although the Nb-O bond length and O K-edge XAS lineshape are reportedly sensitive to d_{z^2} occupancy,^{14,17,27} direct measurement of Li concentration combined with accurate simulations of the O K-edge XAS are required to fully verify the electronic structure evolution of Li_xNbO_2 and understand the memristive mechanism.

To evaluate the quality of our pristine LiNbO_2 crystals, powder x-ray diffraction (XRD) was performed. Figure 2(a) shows the hexagonal $P6_3/mmc$ crystal structure (inset) and XRD pattern of our LiNbO_2 powder with the reflections indexed with PDF 029-0815. The XRD pattern predominantly shows the expected structure with some negligible contribution from LiNbO_3 impurities, which were likely introduced during the powder preparation process. XPS studies confirmed that these impurities were mainly limited to the crystal surface and could be reduced by exposing fresh crystal surfaces using a razor blade (see section II A. of the supplementary material). Henceforth, all results shown were taken on carefully cleaved samples and/or measured using bulk-sensitive techniques to avoid spectral contamination from over-oxidized surface species.

Bulk-sensitive extended x-ray absorption fine structure (EXAFS) of lithium niobite ground pellets was performed to confirm the local atomic structure, shown in Figure 2(b). The data was fit using the LiNbO_2 crystal structure from the materials project database (ICSD-451)²⁸ (see section II B. of the supplementary materials). The first peak around 1.654 \AA corresponds to the Nb-O interaction in the first coordination shell, while the second peak around 2.596 \AA is due to the Nb-Nb interaction in the second coordination shell. Excellent agreement between the experimental data and theory is achieved up to $\sim 5 \text{ \AA}$.

HAXPES was then employed to confirm the bulk Nb oxidation states of our lithium niobite crystals, shown in Figure 2(c). NbO_2 and Nb_2O_5 thin films are used as Nb^{4+} and Nb^{5+} oxidation state references. The Nb 3d spectra consists of two distinct spin-split peaks ($3d_{5/2}$ and $3d_{3/2}$), with the energetic positions of the primary $3d_{5/2}$ peak at

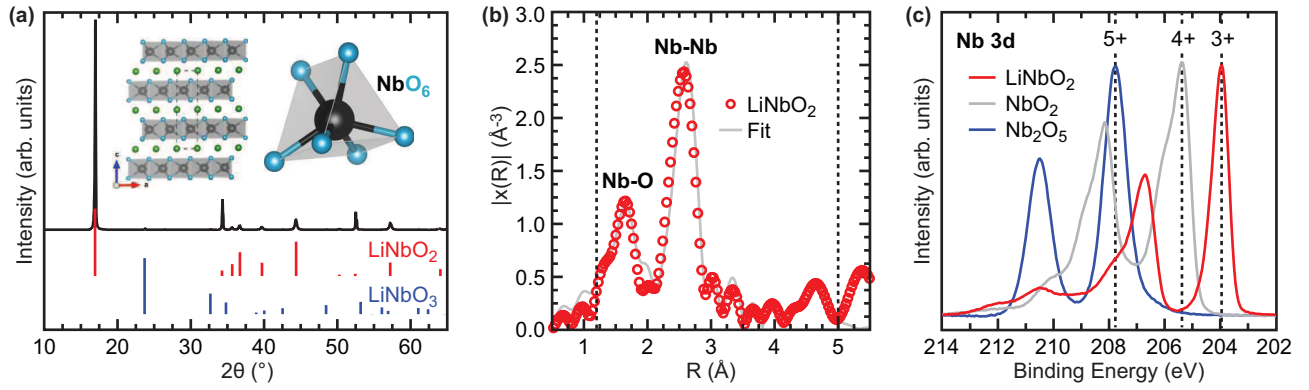


FIG. 2. (a) X-ray diffraction and (b) EXAFS fit. The fitting range is denoted by the dashed lines. (c) HAXPES (6 keV) of pristine LiNbO_2 single crystals compared with NbO_2 (Nb^{4+}) and Nb_2O_5 (Nb^{5+}) references, confirming the expected Nb^{3+} oxidation state of LiNbO_2 . Dashed vertical lines indicate energetic positions of the Nb $3d_{5/2}$ peak for each oxidation state.

204.1 eV, 206.7, and 207.3 for Nb^{3+} , Nb^{4+} and Nb^{5+} , respectively.^{15,29–34} Our pristine LiNbO_2 displays no evidence of Nb^{4+} , however, it does display a weak Nb^{5+} -like component consistent with there being an over-oxidized LiNbO_3 surface. Taken together, the XRD, EXAFS, and HAXPES results confirm the overall phase purity of our LiNbO_2 crystals.

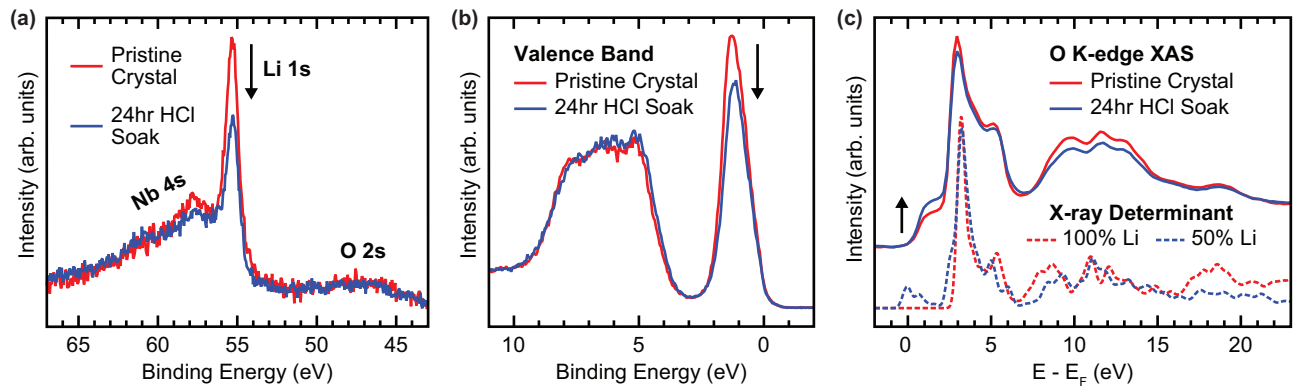


FIG. 3. Soft XPS of the (a) Li 1s core level and (b) valence band region, as well as (c) TEY mode O K-edge XAS compared with x-ray determinant approach simulations for pristine and 24 hour HCL soaked LiNbO_2 crystals.

The effect of chemical delithiation on the electronic structure of LiNbO_2 was studied via more surface sensitive XPS and XAS, as shown in Figure 3. The lower photon energy ($h\nu = 700$ eV) used for the XPS results in a higher Li 1s photo-ionization cross section than is possible with a traditional laboratory-based XPS system, thus improving our sensitivity to variations in Li content associated with delithiation (see section II C. of the supplementary materials). After the crystal was soaked for 24 hours in an HCl bath, a drop in the Li 1s peak intensity is observed in Figure 3(a), associated with a reduction in bulk Li content. This delithiation is accompanied by a compensating change to a higher Nb oxidation state observed in both the Nb 4s and 3d core regions, as well as a reduced Nb-O bond length in EXAFS fitting and a shifted Nb K-edge XANES spectra (see section II B. of the supplementary materials). This delithiation also results in the depopulation of Nb states near the Fermi level, as shown in Figure 3(b). Importantly, the lack of a clear Fermi edge upon delithiation indicates that the material stays within p -type semiconductor regime, i.e., not fully metallic.

Figure 3(c) shows experimental O K-edge spectra taken using TEY mode XAS and simulations of the O K-edge calculated using the x-ray formalism of the core-hole approach.²² One feature that clearly changes with lithium content is a pre-edge feature located around 1 - 2 eV, which is found to increase in intensity with delithiation. While simulations show a complete lack of this pre-edge feature at 100% lithiation, our pristine experimental spectra still displays some weight at this energy, indicating the pristine single crystals may not possess a 100% lithium concentration. This is somewhat expected, considering our LPEE growth requires dissolution and cleaning in a DI water bath, and DI water has been previously reported to remove 10-11% of the lithium from LiNbO_2 .³⁵ It is also important to note that our O

K-edge lineshapes are in agreement with those previously reported by Greenlee et al. from spatially resolved in-situ O K-edge XAS of LiNbO_2 devices. This indicates that perfectly stoichiometric LiNbO_2 is not necessary to achieve a memristive response.¹⁴ Additionally, the trends Greenlee et al. observed across their device from the positive to negative electrode match our observed changes with delithiation, confirming that changing Li content produces the observed analog memristive response.

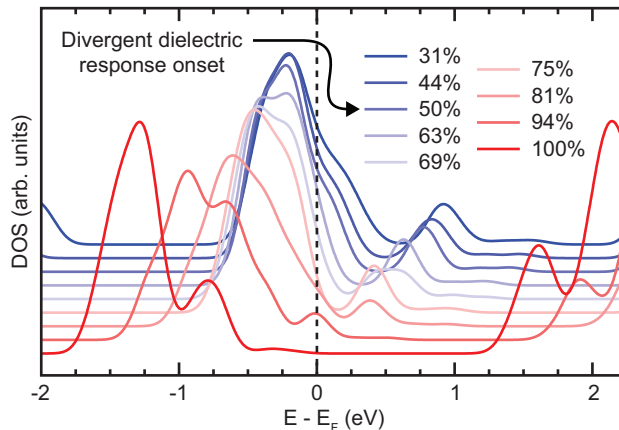


FIG. 4. Evolution of the density of states as function of x in Li_xNbO_2 . A continuously increasing hole population was observed with decreasing Li.

Additional computational methods were used to qualitatively estimate the regime of p -type doping observed in our samples. Figure 4 shows the projected density of states of Li_xNbO_2 as a function of Li content. Starting with the stoichiometric $x = 100\%$ case, the semiconducting gap is generated the Nb d manifold splitting of ~ 1.5 eV. While the experimental gap is closer to 2 eV¹⁷, this is consistent with other theoretical predictions^{27,36} and the general tendency of LDA methods to under-estimate gap strengths.

Looking at the first principles simulations for delithiated cases ($x < 100\%$), we can now clarify the electronic response without assuming a rigid band model. As Li is driven out of the system, there is a clear auto-doping effect where the top of the valence band is heavily p -doped as previously reported,¹⁷ however, the band curvature is still high at marginal delithiation and only flattens out upon deeper delithiation. The onset of a divergent dielectric function, meaning the onset of metallicity, is not predicted to occur until nearly 50% delithiation (see section II D. of the supplementary material). This indicates the formation of light hole states, namely the depopulation of d_{z^2} observed in operando O K-edge XAS,¹⁴ can give rise to the low field analog memristive response before truly metallic behavior sets in.

By comparing the measured valence band spectra (Fig. 3(b)) to simulations and operando XAS studies of active layers, we conclude that the memristive response is due to lithium variation within the p -type semiconductor (marginal delithiation) regime. We also conclude that the memristive response does not require the metallic phase (Fig. 4), suggesting the dominant turn-on effect is instead the formation of light p -carriers. In that regard, although the migration of lithium ions within LiNbO_2 is not confined within pre-formed filaments, the memristive mechanism is similar to that of some filamentary memristors investigated using XAS wherein the migration of oxygen ions modulates the conductivity of the semiconducting active layer.^{16,37} However, in the case of LiNbO_2 , the more uniform Li diffusion throughout the active layer results in a much more gradual (analog) conductivity response than is observed in traditional filamentary memristors.

CONCLUSION

In conclusion, the analog memristive behavior observed in Li_xNbO_2 single crystals has been investigated using a variety of experimental and theoretical techniques. We show intrinsic memristive behavior in lithium niobite phase-pure single crystals, and use chemical delithiation of these crystals to benchmark the observed bias-induced electronic structure changes. We show that removal of Li^+ oxidizes the Nb and thus depopulates the top Nb d -states within the valence band, facilitating the onset of p -type conduction prior to metallicity. This work clarifies that the field driven Li-ion motion inherent to Li_xNbO_2 is a viable analog switching mechanism that does not require any complex interfacial effects or pre-forming/electroforming to function.

SUPPLEMENTARY MATERIAL

See supplementary material for further details on the experimental and theoretical methodologies, as well as additional supporting data including EXAFS fitting results, XPS taken at multiple photon energies, and calculations of the dielectric tensor as a function of Li content.

ACKNOWLEDGMENTS

This material is based upon work supported by the Air Force Office of Scientific Research under award number FA9550-18-1-0024. Galo J. Paez acknowledges doctoral degree grant support from the Fulbright Foreign Student Program (Grant ID: E0565514) and Keith Tirpak was supported by a NSF-REU (NSF DMR-1658990). We acknowledge Diamond Light Source for time on Beamline I09 under Proposals SI20647. This research used resources of the Center for Functional Nanomaterials and the National Synchrotron Light Source II, which are U.S. Department of Energy (DOE) Office of Science facilities at Brookhaven National Laboratory, under Contract No. DE-SC0012704. This research used resources of the Advanced Light Source and the Molecular Foundry, which are U.S. DOE Office of Science facilities at Lawrence Berkeley National Laboratory under Contract No. DE-AC02-05CH11231. This research used resources of the Advanced Photon Source, a U.S. DOE Office of Science User Facility operated for the DOE Office of Science by Argonne National Laboratory under Contract No. DE-AC02-06CH11357; additional support by National Science Foundation under Grant no. DMR-0703406.

- ¹T. Prodromakis and C. Toumazou, "A review on memristive devices and applications." in *ICECS* (2010) pp. 934–937.
- ²C. Sung, H. Hwang, and I. K. Yoo, "Perspective: A review on memristive hardware for neuromorphic computation," *Journal of Applied Physics* **124**, 151903 (2018).
- ³E. Chicca, G. Indiveri, and R. Douglas, "An adaptive silicon synapse," in *Proceedings of the 2003 International Symposium on Circuits and Systems, 2003. ISCAS '03.* (IEEE, 2003).
- ⁴W. M. Holt, "1.1 Moore's law: A path going forward," in *Solid-State Circuits Conference (ISSCC), 2016 IEEE International* (IEEE, 2016) pp. 8–13.
- ⁵Y. Li, Z. Wang, R. Midya, Q. Xia, and J. J. Yang, "Review of memristor devices in neuromorphic computing: materials sciences and device challenges," *Journal of Physics D: Applied Physics* **51**, 503002 (2018).
- ⁶D. Kuzum, S. Yu, and H. P. Wong, "Synaptic electronics: materials, devices and applications," *Nanotechnology* **24**, 382001 (2013).
- ⁷I. A. Young and D. E. Nikonov, "Principles and trends in quantum nano-electronics and nano-magnetics for beyond-CMOS computing," in *Solid-State Device Research Conference (ESSDERC), 2017 47th European* (IEEE, 2017) pp. 1–5.
- ⁸J. J. Yang, M. D. Pickett, X. Li, D. A. Ohlberg, D. R. Stewart, and R. S. Williams, "Memristive switching mechanism for metal/oxide/metal nanodevices," *Nature nanotechnology* **3**, 429 (2008).
- ⁹T. Prodromakis, C. Toumazou, and L. Chua, "Two centuries of memristors," *Nature Materials* **11**, 478–481 (2012).
- ¹⁰J. J. Yang, D. B. Strukov, and D. R. Stewart, "Memristive devices for computing," *Nature nanotechnology* **8**, 13 (2013).
- ¹¹M. J. Geselbracht, T. J. Richardson, and A. M. Stacy, "Superconductivity in the layered compound Li_xNbO_2 ," *Nature* **345**, 324 (1990).
- ¹²J. D. Greenlee, W. L. Calley, W. Henderson, and W. A. Doolittle, "Halide based mbe of crystalline metals and oxides," *physica status solidi c* **9**, 155–160 (2012), <https://onlinelibrary.wiley.com/doi/pdf/10.1002/pssc.201100468>.
- ¹³J. D. Greenlee, W. L. Calley, M. W. Moseley, and W. A. Doolittle, "Comparison of interfacial and bulk ionic motion in analog memristors," *IEEE Transactions on Electron Devices* **60**, 427–432 (2013).
- ¹⁴J. D. Greenlee, C. F. Petersburg, W. Laws Calley, C. Jaye, D. A. Fischer, F. M. Alamgir, and W. Alan Doolittle, "In-situ oxygen x-ray absorption spectroscopy investigation of the resistance modulation mechanism in LiNbO_2 memristors," *Applied Physics Letters* **100**, 182106 (2012).
- ¹⁵J. C. Shank, M. B. Telekamp, M. J. Wahila, S. Howard, A. S. Weidenbach, B. Zivasatienraj, L. F. Piper, and W. A. Doolittle, "Scalable Memdiodes Exhibiting Rectification and Hysteresis for Neuromorphic Computing," *Scientific reports* **8**, 12935 (2018).
- ¹⁶S. Kumar, Z. Wang, X. Huang, N. Kumari, N. Davila, J. P. Strachan, D. Vine, A. L. D. Kilcoyne, Y. Nishi, and R. S. Williams, "Oxygen migration during resistance switching and failure of hafnium oxide memristors," *Applied Physics Letters* **110**, 103503 (2017).
- ¹⁷J. C. Shank, M. B. Telekamp, and W. A. Doolittle, "Evidence of ion intercalation mediated band structure modification and opto-ionic coupling in lithium niobate," *Journal of Applied Physics* **117**, 035704 (2015).
- ¹⁸Y. Liang and D. Prendergast, "Quantum many-body effects in x-ray spectra efficiently computed using a basic graph algorithm," *Phys. Rev. B* **97**, 205127 (2018).
- ¹⁹J. D. Greenlee, J. C. Shank, M. B. Telekamp, B. P. Gunning, C. A. Fabien, and W. A. Doolittle, "Liquid phase electro-epitaxy of memristive LiNbO_2 crystals," *Crystal Growth & Design* **14**, 2218–2222 (2014).
- ²⁰F. Lin, I. M. Markus, D. Nordlund, T.-C. Weng, M. D. Asta, H. L. Xin, and M. M. Doeff, "Surface reconstruction and chemical evolution of stoichiometric layered cathode materials for lithium-ion batteries," *Nature communications* **5**, 3529 (2014).
- ²¹G. Kresse and J. Furthmüller, "Efficient iterative schemes for ab initio total-energy calculations using a plane-wave basis set," *Phys. Rev. B* **54**, 11169–11186 (1996).
- ²²Y. Liang, J. Vinson, S. Pemmaraju, W. S. Drisdell, E. L. Shirley, and D. Prendergast, "Accurate X-Ray Spectral Predictions: An Advanced Self-Consistent-Field Approach Inspired by Many-Body Perturbation Theory," *Phys. Rev. Lett.* **118**, 096402 (2017).
- ²³P. Giannozzi, S. Baroni, N. Bonini, M. Calandra, R. Car, C. Cavazzoni, D. Ceresoli, G. L. Chiarotti, M. Cococcioni, I. Dabo, A. Dal Corso, S. de Gironcoli, S. Fabris, G. Fratesi, R. Gebauer, U. Gerstmann, C. Gougoussis, A. Kokalj, M. Lazzeri, L. Martin-Samos, N. Marzari, F. Mauri, R. Mazzarello, S. Paolini, A. Pasquarello, L. Paulatto, C. Sbraccia, S. Scandolo, G. Sclauzero, A. P. Seitsonen, A. Smogunov, P. Umari, and R. M. Wentzcovitch, "QUANTUM ESPRESSO: a modular and open-source software project for quantum simulations of materials," *Journal of Physics: Condensed Matter* **21**, 395502 (2009).

- ²⁴P. Giannozzi, O. Andreussi, T. Brumme, O. Bunau, M. B. Nardelli, M. Calandra, R. Car, C. Cavazzoni, D. Ceresoli, M. Cococcioni, N. Colonna, I. Carnimeo, A. D. Corso, S. de Gironcoli, P. Delugas, R. A. D. Jr, A. Ferretti, A. Floris, G. Fratesi, G. Fugallo, R. Gebauer, U. Gerstmann, F. Giustino, T. Gorni, J. Jia, M. Kawamura, H.-Y. Ko, A. Kokalj, E. Kkbenli, M. Lazzeri, M. Marsili, N. Marzari, F. Mauri, N. L. Nguyen, H.-V. Nguyen, A. O. de-la Roza, L. Paulatto, S. Ponc, D. Rocca, R. Sabatini, B. Santra, M. Schlipf, A. P. Seitsonen, A. Smogunov, I. Timrov, T. Thonhauser, P. Umari, N. Vast, X. Wu, and S. Baroni, “Advanced capabilities for materials modelling with QUANTUM ESPRESSO,” *Journal of Physics: Condensed Matter* **29**, 465901 (2017).
- ²⁵J. D. Greenlee, J. C. Shank, M. B. Tellekamp, E. X. Zhang, J. Bi, D. M. Fleetwood, M. L. Alles, R. D. Schrimpf, and W. A. Doolittle, “Radiation effects on LiNbO₂ memristors for neuromorphic computing applications,” *IEEE Transactions on Nuclear Science* **60**, 4555–4562 (2013).
- ²⁶J. C. Shank, M. B. Tellekamp, and W. A. Doolittle, “The crystallization and properties of sputter deposited lithium niobite,” *Thin Solid Films* **609**, 6 – 11 (2016).
- ²⁷E. R. Ylvisaker and W. E. Pickett, “First-principles study of the electronic and vibrational properties of LiNbO₂,” *Physical Review B* **74**, 075104 (2006).
- ²⁸A. Jain, S. P. Ong, G. Hautier, W. Chen, W. D. Richards, S. Dacek, S. Cholia, D. Gunter, D. Skinner, G. Ceder, and K. a. Persson, “The Materials Project: A materials genome approach to accelerating materials innovation,” *APL Materials* **1**, 011002 (2013).
- ²⁹I. Goldfarb, D. Ohlberg, J. Strachan, M. Pickett, J. J. Yang, G. Medeiros-Ribeiro, and R. Williams, “Band offsets in transition-metal oxide heterostructures,” *Journal of Physics D: Applied Physics* **46**, 295303 (2013).
- ³⁰X. Jia, L. Kang, X. Liu, Z. Wang, B. Jin, S. Mi, J. Chen, W. Xu, P. Wu, *et al.*, “High performance ultra-thin niobium films for superconducting hot-electron devices,” *IEEE Trans. Appl. Supercond* **23**, 2300704–2300704 (2013).
- ³¹Y. Wang, R. B. Comes, S. Kittiwatanakul, S. A. Wolf, and J. Lu, “Epitaxial niobium dioxide thin films by reactive-biased target ion beam deposition,” *Journal of Vacuum Science & Technology A: Vacuum, Surfaces, and Films* **33**, 021516 (2015).
- ³²Q.-Y. Hao, B.-C. Zhu, D.-K. Wang, S.-Y. Zeng, Z. Gao, Y.-W. Hu, Y. Wang, Y.-K. Wang, and K.-B. Tang, “A New Potassium Intercalation Compound of 3R-Nb_{1.1}S₂ and its Superconducting Hydrated Derivative Synthesized via Soft Chemistry Strategy,” *Chemistry Select* **1**, 2610–2616 (2016).
- ³³C. Dong, X. Wang, X. Liu, X. Yuan, W. Dong, H. Cui, Y. Duan, and F. Huang, “In situ grown Nb₄N₅ nanocrystal on nitrogen-doped graphene as a novel anode for lithium ion battery,” *RSC Advances* **6**, 81290–81295 (2016).
- ³⁴S. B. Basuvalingam, B. Macco, H. C. Knoops, J. Melskens, W. M. Kessels, and A. A. Bol, “Comparison of thermal and plasma-enhanced atomic layer deposition of niobium oxide thin films,” *Journal of Vacuum Science & Technology A: Vacuum, Surfaces, and Films* **36**, 041503 (2018).
- ³⁵E. G. Moshopoulou, P. Bordet, and J. J. Capponi, “Superstructure and superconductivity in Li_{1-x}NbO₂ ($x \approx 0.7$) single crystals,” *Physical Review B* **59**, 9590–9599 (1999).
- ³⁶D. L. Novikov, V. A. Gubanov, V. G. Zubkov, and A. J. Freeman, “Electronic structure and electron-phonon interactions in layered Li_xNbO₂ and Na_xNbO₂,” *Phys. Rev. B* **49**, 15830–15835 (1994).
- ³⁷C. Baeumer, C. Schmitz, A. Marchewka, D. N. Mueller, R. Valenta, J. Hackl, N. Raab, S. P. Rogers, M. I. Khan, S. Nemsak, M. Shim, S. Menzel, C. M. Schneider, R. Waser, and R. Dittmann, “Quantifying redox-induced Schottky barrier variations in memristive devices via in operando spectromicroscopy with graphene electrodes,” *Nature Communications* **7**, 1–7 (2016).